Hexaborides: Materials of diverse physics

Steffen Wirth[#], Maria Victoria Ale Crivillero, Horst Borrmann, Hubert Dawczak-Dębicki, Lin Jiao, Deepa Kasinathan, Sahana Rößler, Frank Steglich

The hexaborides constitute a class of materials, which exhibit highly interesting properties. The Kondo insulator SmB_6 is considered the prototype candidate material in which an interplay of strong electron correlations and non-trivial topology can be studied. We continued our efforts towards establishing the topological nature of the surface states by studying magnetically substituted SmB_6, and by employing spin-polarized tunneling. Using tunneling spectroscopy, the formation of magnetic polarons in EuB_6 could be visualized for the first time. In all these studies, atomically flat surface areas and their unambiguous assignment of the surface termination on *in situ* cleaved samples is an indispensable prerequisite.

Cubic hexaborides are known for more than a century [1] and their structure of type CaB_6 ($Pm\overline{3}m$) [2] constitutes a very versatile class of compounds [3]. They typically feature high melting points, high hardness and excellent chemical stability. LaB_6 features a very low work function of about 2.7 eV [4] and therefore, is an established cathode material. In contrast, electron-doped CaB_6 is a ferromagnetic material, albeit with a low magnetic moment [5], and CeB_6 exhibits quadrupolar ordering [6]. The hexaborides with trivalent rare-earths are typically highly conductive. From Hall measurements, it was shown [7] that these hexaborides have one charge carrier per rare-earth atom, i.e. the B-octahedra take up two electrons. In line with this, the hexaborides based on divalent Yb and Eu exhibit very low charge carrier densities, with EuB_6 showing complex ferromagnetic order [8,9]. The noted exception to this valence rule is SmB_6 exhibiting intermediate valence, see e.g. [10,11]. SmB_6 is still under intense scrutiny for its surface termination after cleaving [12,13] and, above all, the possible topologically nature of the metallic surface state [14,15].

In continuation of our earlier work [11,16,17,18] on SmB_6 we focused on these issues. We addressed the surface termination in detail [19,20] and studied the impact of Gd-substitution and tunneling with magnetic tips on the surface state of SmB_6 [21]. For the ferromagnetic semimetal EuB_6 [22,23] the formation of magnetic polarons has been unequivocally visualized.

Assignment of surface termination in hexaborides

(*Steffen Wirth, Sahana Rößler, Lin Jiao, Maria Victoria Ale Crivillero, Priscila F. S. Rosa and Zachary Fisk* [19])

For many surface sensitive studies like ARPES or STM, clean sample surfaces are typically produced by *in situ* cleaving. From the comparatively simple structure one might expect either B or rare earth (*RE*) terminated atomically flat surfaces. However, the vast majority of the surface areas exhibits roughnesses on

the nm scale. In addition, surface reconstructions are encountered, typically of the (2×1) type, which are energetically more favorable compared to the (1×1) polar surfaces [17]. Moreover, the inter-octahedral B distance is slightly shorter than the intra-octahedral one and hence, cleaving may also involve intra-octahedral bond breaking. In consequence, atomically flat surface areas as shown in Fig. 1 are extremely rarely observed; on some of our more than 40 cleaved sample surfaces, we did not find any atomically flat area even after weeks of searching.

The cubic structure of the hexaborides does not allow for a straightforward distinction of the different surface terminations, especially for atomically flat surfaces [20]. This has led to some ambiguity in the assignment of the different terminations [12,13]. To resolve this issue, we searched for a step on an otherwise flat surface that involves both, a B- and a *RE*-termination, as presented in Fig. 2(a). We note that in our study of the hexaborides, which runs for almost a decade by now, we only encountered two such incidences emphasizing the importance of acquiring sufficient statistics.

Just by keeping the crystallographic orientation of the cleaved single crystal SmB_6 surface of Fig. 2(a) in mind (white arrows), it is obvious that different termi-
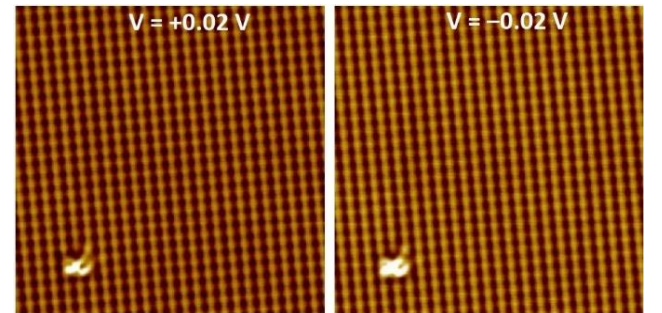
Fig. 1: Clean, B-terminated surface of SmB_6 of areas 10 x 10 nm^2 obtained in dual-bias mode. V_b = +0.02 V (left) and -0.02 V (right), I_{sp} = 0.3 nA, T = 1.7 K. The total height scale is 90 pm. From [19].
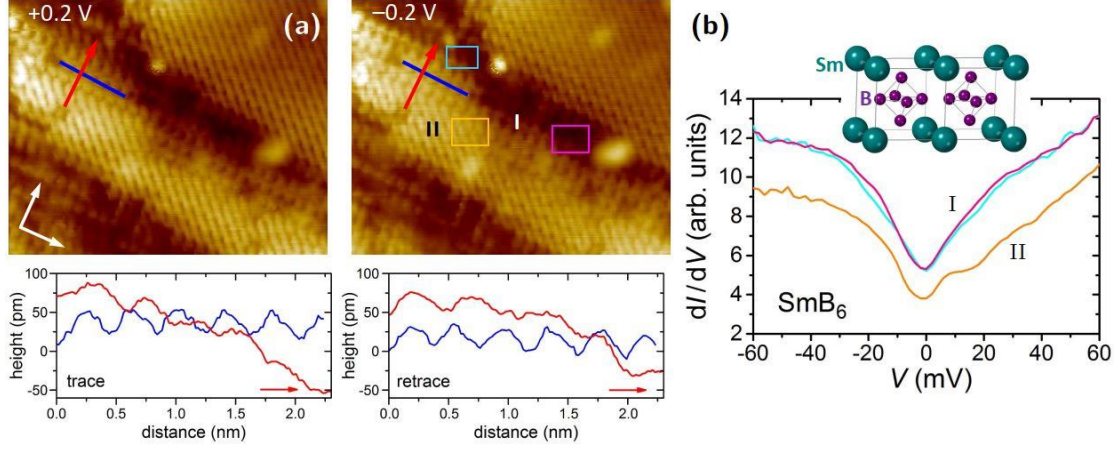
Fig. 2: (a) SmB₆ topography of an area of 10 x 8 nm² exhibiting both Sm- and B-terminated areas. The images were obtained in dual-bias mode: V_b = +0.2 V (left) and V_b = -0.2 V (right). The height scans were taken along the lines of corresponding color in the topography images. Along the direction of the red arrows the sample height decreases by about 100–130 pm. The white arrows indicate the main crystallographic directions ⟨100⟩ and ⟨010⟩, respectively. The colored rectangles mark the areas over which the spectroscopy curves in (b) were averaged. (b) Tunneling spectroscopies obtained on B (marked I) and Sm (marked II) terminated areas. V_b = +0.2 V, I_{sp} = 0.6 nA, V_{mod} = 1 mV, T ≈ 6 K. The inset exhibits two adjacent unit cells of the cubic SmB₆ lattice. After [19].

nations are encountered. Some protrusions are aligned along the main [100] crystallographic directions (cf. the blue scan line and area marked I), while other runs along the diagonal [110] (e.g. area marked II). The blue height scan along [100] indicates protrusions with distances corresponding nicely to the lattice constant a = 4.133 Å. The scans taken along the red arrow exhibit height changes much smaller than a, and less obvious corrugations, possibly related to crystallographic imperfections within such regions of changing overall height. Obviously, the only consistent assignment is by areas II representing Sm terminations, and areas I such of B-terminations, cf. inset to Fig. 2(b): i) The height change along the red arrows is then expected to be ~100 pm. ii) For the Sm-terminated surfaces II, in addition to the Sm atoms the apex atoms of the B-octahedra are seen, which gives rise to the corrugations running along the diagonal [110] directions within these areas [16,17].

The tunneling spectra shown in Fig. 2(b) can now unambiguously be assigned to B- (areas I) and Sm-terminations (areas II). The spectra are averaged over the areas marked by corresponding colors in Fig. 2(a). Clearly, there is an additional peak at around 5 mV in case of a Sm-termination as reported earlier [16]. It should be noted that the different values V_b do not significantly change the spectroscopies in Fig. 2(a).

Topological nature of surface states in SmB₆ (*Lin Jiao, Sahana Rößler, Deepa Kasinathan, Priscila F. S.*

Rosa, Chunyu Guo, Huiqiu Yuan, Chao-Xing Liu, Zachary Fisk, Frank Steglich and Steffen Wirth [21])

The existence of metallic states on SmB₆ surfaces is well established by now, while their topological origin is still a matter of debate [14]. To scrutinize the topological nature of the surface states, we set off to study the impact of magnetic impurities in SmB₆. Such impurities are expected to break time reversal symmetry, which should strongly suppress the surface states if they are topological in nature. We investigated lightly Gd-substituted and, for comparison with a non-magnetic analogue, Y-substituted SmB₆.

In Figs. 3(a)–(c), topographies of pure SmB₆, 3% Y-substituted and 0.5% Gd-substituted SmB₆ are presented. In all likelihood, the impurities seen in Figs. 3(b) and (c) are Y and Gd atoms, respectively (see Supplementary Materials to [21]). In the following, we study the evolution of the spectra as we approach the respective impurities, Fig. 3(d)–(f). Away from any impurity, the spectra (labelled #5/#6) compare nicely to those obtained on pristine and clean SmB₆ [18]. As outlined in [18], the peak at around -6.5 mV, which contains a significant surface contribution at T = 0.35 K, dominates the spectra. Upon approaching the impurities, this peak is reduced (all spectra labelled #1 were taken on top of the respective impurity). The peak heights as a function of distance from the impurity, which is located at position 0, are presented in Figs. 3(g)–(i). In pure SmB₆, the peak height
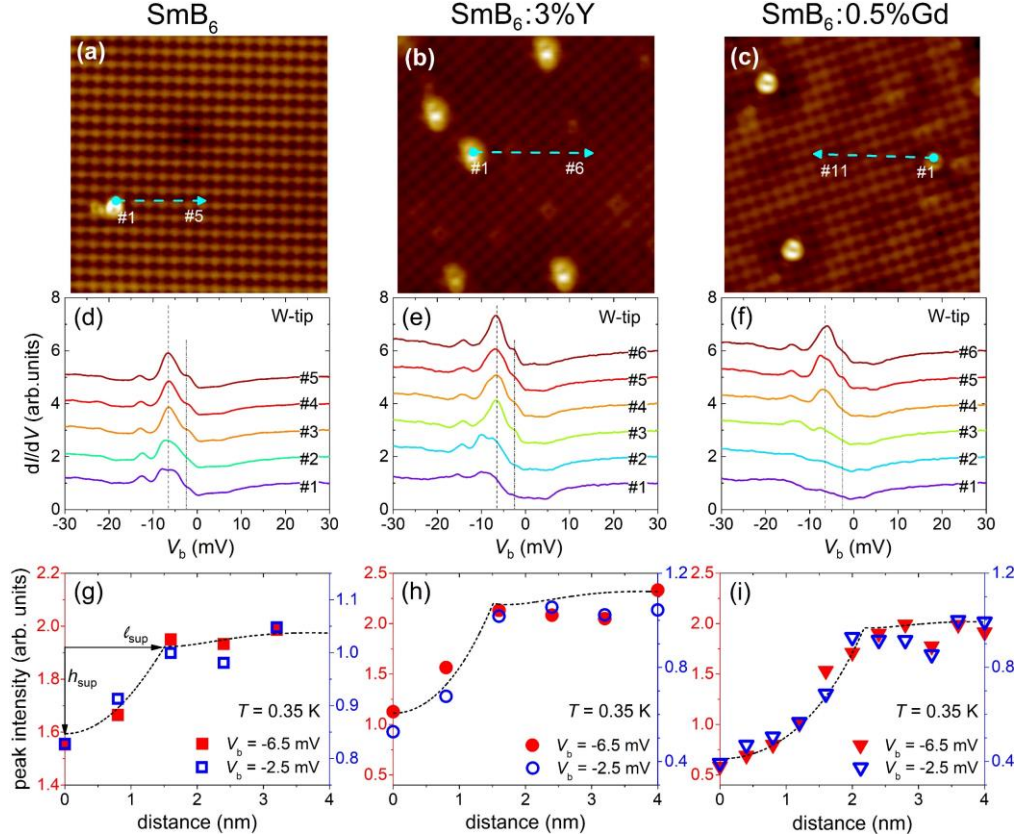
Fig. 3: (a)–(c) Topographies (8 nm × 8 nm) of pure SmB₆ as well as SmB₆:3%Y and SmB₆:0.5%Gd. (d)–(f) dI/dV curves of the three samples measured at 0.35 K. The curves were measured at positions with increasing distance from the impurity (the impurities are located at #1) along the cyan arrows in (a)–(c), respectively (V_b = +30 mV; I_{sp} = 0.1 nA). (g)–(i) dI/dV values at V_b = −6.5 meV (red) and −2.5 meV (blue) with increasing distance from the impurity (impurities are located at 0). The black dashed lines are fits according to the model. h_{sup} and ℓ_{sup} indicate the suppression of peak intensities at the impurities and its lateral extents, respectively. From [21].

at -6.5 mV is only slightly reduced at the impurity site, and somewhat more at an Y atom in SmB₆:3%Y. In contrast, there is no signature of such a peak left at the Gd impurity in SmB₆:0.5%Gd, see spectrum #1 in Fig. 3(f). This implies that the signature peak of the surface states is largely suppressed in Gd-substituted SmB₆. The remaining spectral weight around -6.5 mV results likely from a bulk contribution [18]. Moreover, the suppression of the -6.5 mV-peak in SmB₆:0.5%Gd is larger in extent: the unperturbed peak height is recovered at a distance ℓ_{sup} ≈ 2.2 nm, compared to ℓ_{sup} ≈ 1.5 nm for pure SmB₆ and SmB₆:3%Y. Consequently, the suppression of the surface state is more pronounced in strength and extend for magnetic (Gd) impurities. The fact that such a suppression is also seen in pure SmB₆ and for non-magnetic Y-substitution in SmB₆:3%Y is likely related to the Kondo-hole effect. The larger ℓ_{sup} upon Gd substitution has direct implications for the resistivity: the larger areas of suppressed surface states cluster to one another already at 3% Gd substitution and impede a percolating surface conduction path. In turn, the low-T resistivity

plateau – the hallmark of the metallic surface state – does not form.
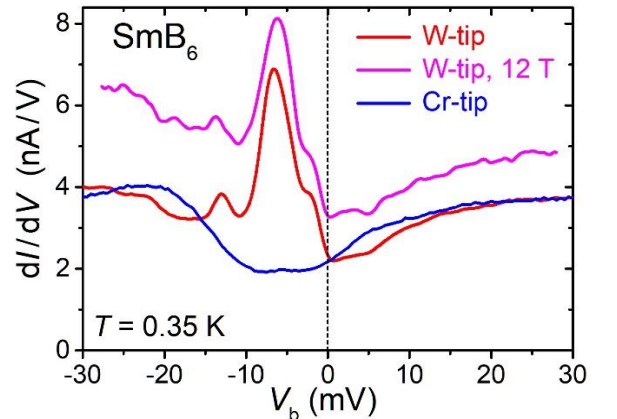
Fig. 4: Tunneling Spectra obtained on nonreconstructed surfaces of pure SmB₆ by using a W tip (red) and a magnetic Cr tip (blue) at 0.35 K and zero magnetic field. For comparison, a spectrum taken with a W tip at $\mu_0 H$ = 12 T is presented (pink, vertically offset by 1 nA/V). V_b = 50 mV; I_{sp} = 200 pA, V_{mod} = 0.3 mV. From [21].

3

In order to describe the above findings, a model was adopted in which the Dirac electrons of the topological surface state are assumed to be locally coupled to a magnetic impurity through exchange interaction [21]. Fitting such a model to our data resulted in the dotted lines in Figs. 3(G–I) and values ℓ_{sup} as given above. Estimates of the Fermi velocity of the Dirac electrons $v_F \approx 3000$ ms^{-1} and of the position of the Dirac cone at -5 meV agree well with data in [15].

The substitution of Y or Gd in SmB$_6$, however, may give rise to modified bulk properties. To avoid this, we conducted tunneling spectroscopy using magnetic Cr tips. The peak at -6.5 mV characteristic of the surface states is again suppressed (Fig. 4), similar to our observations near Gd-substitutions in SmB$_6$:0.5%Gd. This clearly supports our interpretation of suppressed surface states through magnetic exchange interaction.

Visualization of polaron formation in EuB$_6$ (*Merlin Pohlit, Sahana Rößler, Yuzo Ohno, Hideo Ohno, Stephan von Molnár, Zachary Fisk, Jens Müller and Steffen Wirth* [22])

Materials in which the electronic and magnetic properties of the system are strongly modified by the exchange coupling between the conduction electrons and local magnetic moments are not only of fundamental importance in modern condensed-matter physics, but also of technological interest, e.g., in spintronics research. One such coupling of particular interest is related to the formation of ordered magnetic clusters, or magnetic polarons, which give rise to intrinsically inhomogeneous states. Within the magnetic polaron, the charge carriers to localize while spin-polarizing the local magnetic moments over a finite distance. Once the magnetic polarons overlap, the charge carriers can suddenly delocalize, resulting in a mobility increase. This intriguingly simple model can explain the colossal magnetoresistance (CMR) effect in many materials.

In an effort to directly visualize the electronic phase separation involved in the polaron formation, and find evidence for magnetic cluster formation in finite magnetic fields, we have chosen to investigate the ferromagnetic semimetal EuB$_6$. It exhibits a strong CMR effect near the ferromagnetic transition temperature $T_{c1} = 15.3$ K [8], at which the magnetic polarons are believed to percolate. The magnetic polarons start forming at around $T^* \sim 35 - 40$ K, and finally merge at $T_{c2} = 12.6$ K [9].

Scanning tunneling spectroscopy is a well-suited tool for studying the local density of states (DOS) at an
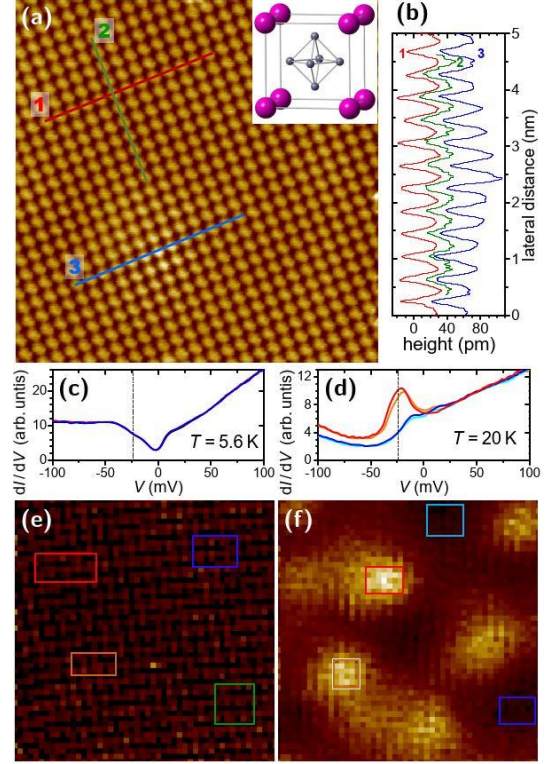
Fig. 5: (a) Topography of EuB$_6$ over an area of 10 nm × 10 nm. (b) Height scans along the lines marked in (a). (c),(d) dI/dV-spectra at 5.6 K and 20 K, averaged within areas marked in (e) and (f), respectively, by rectangles of corresponding colors. In (c), a curve averaged over the total area is also included. (e),(f) Local conductance maps at $V_b = -24$ mV over an area of 20 × 20 nm^2 at 5.6 K and 20 K. At 20 K, local inhomogeneities are most pronounced at $V_b = -24$ mV (dashed line in (d)) and clearly visible in (f). Adapted from [22].

atomic length scale and at different temperatures. However, to distinguish electronic from possible structural and/or chemical inhomogeneities, well cleaved surface areas are again an essential prerequisite [23]. A clean and atomically flat surface area of EuB$_6$ is presented in Fig. 5(a) and corresponds to a B-termination (see above). The corrugations along the scan lines $1 - 3$, Fig. 5(b), are in excellent agreement with the EuB$_6$ lattice constant $a = 0.4185$ nm. In particular, we note that line 2 was taken almost perpendicular to the STM fast scan direction and hence, evidences the excellent surface and measurement quality.

The tunneling conductance $g(V) = dI(V)/dV$ is, within simplifying approximations, proportional to the local DOS. As expected, at $T = 5.6$ K, i.e. well below T_{c2}, $g(V)$ does not indicate any electronic inhomogeneity, Figs. 5(c), (e). In contrast, in the paramagnetic regime at 20 K, areas of enhanced local DOS of about $3 - 4$ nm in extent can clearly be recognized, Fig. 5(f). This

enhancement is most pronounced at energies $V_b \approx$ -24 mV, Fig. 5(d). These areas of higher $g(V)$ are found to coalesce at $T = 15$ K [22], i.e. between T_{c1} and T_{c2}, in line with expectations. Micro-Hall magnetometry showed locally inhomogeneous magnetic stray fields within the same temperature window. Taken together, this clearly supports, and provides direct visualization of, the magnetic polaron scenario (as outlined above) for the magnetic and electronic transport behavior of prototypical EuB_6.

External Cooperation Partners

Priscila F. S. Rosa (Los Alamos National Laboratory, Los Alamos, NM, USA); Zachary Fisk (Department of Physics and Astronomy, University of California, Irvine, CA, USA); Chunyu Guo, Huiqiu Yuan (Center for Correlated Matter, Zhejiang University, Hangzhou, China and Department of Physics, Zhejiang University, Hangzhou, China); Chao-Xing Liu (Department of Physics, The Pennsylvania State University, University Park, PA, USA); Merlin Pohlit, Jens Müller (Institute of Physics, Goethe-University Frankfurt, Germany); Stephan von Molnár (Department of Physics, Florida State University, Tallahassee, FL, USA).

References

[1] *Sur la préparation et les propriétiés des borures de calcium, de strontium et de barium, H. Moissan and P. Williams, C. R. Acad. Sci. (Paris) 125 (1897) 629.*

[2] *The structure of calcium boride, CaB_6, L. Pauling and S. Weinbaum, Z. Kristallogr. 87 (1934) 181.*

[3] *Structure and physical features of the rare-earth borides, J. Etourneau and P. Hagenmuller, Philos. Mag. 52 (1985) 589.*

[4] *Thermoelectric properties of some CaB_6 type hexaborides A. Berrada, A. M. Schroff, J. P. Mercurio, J. Etourneau, and P. Hagenmuller, J. Less-Common Met. 59 (1978) 7.*

[5] *High-temperature weak ferromagnetism in a low-density free-electron gas D. P. Young, D. Hall, M. E. Torelli, Z. Fisk, J. L. Sarrao, J. D. Thompson, H. R. Ott, S. B. Oseroff, and R. G. Goodrich, R. Zysler, Nature 397 (1999) 412.*

[6] *Magnetic phase diagram of CeB_6, J. M. Effantin, J. Rossatmignod, P. Burlet, H. Bartholin, S. Kunii, and T. Kasuya, J. Magn. Magn. Mater. 47–48 (1985) 145.*

[7] *A study of the electronic structure of rare-earth hexaborides, Y. S. Grushko, Y. B. Paderno, K. Y. Mishin, L. I. Molkanov, G. A. Shadrina, E. S. Konovalova, and E. M. Dudnik, Phys. Status Solidi B 128 (1985) 591.*

[8] *Metallization and magnetic order in EuB_6, S. Süllow, I. Prasad, M. C. Aronson, S. Bogdanovich, J. L. Sarrao, and Z. Fisk, Phys. Rev. B 62 (2000) 11626.*

[9] *Magnetically driven electronic phase separation in the semimetallic ferromagnet EuB_6, P. Das, A. Amyan, J. Brandenburg, J. Müller, P. Xiong, S. von Molnár. and Z. Fisk, Phys. Rev. B 86 (2012) 184425.*

[10] *X-ray spectral investigation of samarium hexaboride, E. E. Vainshtein, S. M. Blokhin, and Y. B. Paderno, Soviet Phys.-Solid State 6 (1965) 2318.*

[11] *Bulk and surface electronic properties of SmB_6: a hard x-ray photoelectron spectroscopy study, Y. Utsumi, D. Kasinathan, K.-T. Ko, S. Agrestini, M. W. Haverkort, S. Wirth, Y.-H. Wu, K.-D. Tsuei, D.-J. Kim, Z. Fisk, et al., Phys. Rev. B 96 (2017) 155130.*

[12] *Contrast Reversal in Scanning Tunneling Microscopy and Its Implications for the Topological Classification of SmB_6, H. Herrmann, P. Hlawenka, K. Siemensmeyer, E. Weschke, J. Sánchez-Barriga, A. Varykhalov, N. Y. Shitsevalova, A. V. Dukhnenko, V. B. Filipov, S. Gabáni, et al., Adv. Mat. 32 (2020) 1906725.*

[13] *Consistency between ARPES and STM measurements on SmB_6, C. E. Matt, H. Pirie, A. Soumyanarayanan, Y. He, M. M. Yee, P. Chen, Yu Liu, D. T. Larson, W. S. Paz, J. J. Palacios, et al., Phys, Rev. B 101 (2020) 085142.*

[14] *Samarium hexaboride is a trivial surface conductor, P. Hlawenka, K. Siemensmeyer, E. Weschke, A. Varykhalov, J. Sánchez-Barriga, N. Y. Shitsevalova, A. V. Dukhnenko, V. B. Filipov, S. Gabáni, K. Flachbart, et al., Nat. Commun. 9 (2018) 517.*

[15] *Imaging emergent heavy Dirac fermions of a topological Kondo insulator, H. Pirie, Y. Liu, A. Soumyanarayanan, P. Chen, Y. He, M. M. Yee, P. F. S. Rosa, J. D. Thompson, D.-J. Kim, Z. Fisk, et al., Nat. Phys. 16 (2020) 52.*

[16] *Hybridization gap and Fano resonance in SmB_6, S. Rößler, T.-H. Jang, D.-J. Kim, L. H. Tjeng, Z. Fisk, F. Steglich, and S. Wirth, Proc. Natl. Acad. Sci. USA 111 (2014) 4798.*

[17] *Surface and electronic structure of SmB_6 through Scanning Tunneling Microscopy, S. Rößler, L. Jiao, D.-J. Kim, S. Seiro, K. Rasim, F. Steglich, L. H. Tjeng, Z. Fisk, and S. Wirth, Phil. Mag. 96 (2016) 3262.*

[18] *Additional energy scale in SmB_6 at low temperature, L. Jiao, S. Rößler, D. J. Kim, L. H. Tjeng, Z. Fisk, F. Steglich, and S. Wirth, Nat. Commun. 7 (2016) 13762.*

[19]* *Comparative Scanning Tunneling Microscopy Study on Hexaborides, S. Wirth, S. Rößler, L. Jiao, M. V. Ale Crivillero, P. F. S. Rosa, and Z. Fisk, Phys. Status Solidi B 258 (2021) 2000022.*

[20]* *Phase stability in SmB_6, M. V. Ale Crivillero, S. Rößler, H. Borrmann, H. Dawczak-Debicki, P. F. S. Rosa, Z. Fisk, and S. Wirth, Phys. Rev. Materials 5 (2021) 044202.*

[21]* *Magnetic and defect probes of the SmB_6 surface state, L. Jiao, S. Rößler, D. Kasinathan, P. F. S. Rosa, C. Guo, H. Yuan, C.-X. Liu, Z. Fisk, F. Steglich, and S. Wirth, Sci. Adv. 4 (2018) eaau4886.*

[22]* *Evidence for Ferromagnetic Clusters in the Colossal-Magnetoresistance Material EuB_6, M. Pohlit, S. Rößler, Y. Ohno, H. Ohno, S. von Molnár, Z. Fisk, J. Müller, and S. Wirth, Phys. Rev. Lett. 120 (2018) 257201.*

[23]* *Visualization of localized perturbations on a (001) surface of the ferromagnetic semimetal EuB_6, S. Rößler, L. Jiao, S. Seiro, P. F. S. Rosa, Z. Fisk, U. K. Rößler, and S. Wirth, Phys. Rev. B 101 (2020) 235421.*

_____

[#] wirth@cpfs.mpg.de